arXiv:1404.1603v1 [cond-mat.mes-hall] 6 Apr 2014

Interaction-enhanced electron-hole and valley asymmetries in the lowest Landau level of ABA-stacked trilayer graphene

K. Shizuya
Yukawa Institute for Theoretical Physics
Kyoto University, Kyoto 606-8502, Japan

In a magnetic field graphene trilayers support a special multiplet of 12 zero(-energy)-mode Landau levels with a threefold degeneracy in Landau orbitals. A close look is made into such zero-mode levels in ABA-stacked trilayers, with the Coulomb interaction taken into account. It turns out that the zero-mode Landau levels of ABA trilayers are greatly afflicted with electron-hole and valley asymmetries, which come from general hopping parameters and which are enhanced by the Coulomb interaction and the associated vacuum effect, the orbital Lamb shift, that lifts the zero-mode degeneracy. These asymmetries substantially affect the way the zero-mode levels evolve, with filling, via Coulomb interactions; and its consequences are discussed in the light of experiments.

PACS numbers: 73.22.Pr,73.43.-f,75.25.Dk

I. INTRODUCTION

Graphene, an atomic layer of graphite that supports massless Dirac fermions, displays remarkable and promising electronic properties. Recently there is increasing interest in bilayers and few layers of graphene, where the physics and applications of graphene become richer, with, e.g., a tunable band gap[1–4] for bilayer graphene.

There are some key signatures of Dirac fermions that distinguish graphene from conventional electron systems. (i) In a magnetic field, graphene supports, as the lowest Landau level (LLL), a special set of four zero-energy levels differing in spin and valley, as observed via the half-integer quantum Hall effect. (ii) Graphene is an intrinsically many-body system equipped with the valence band acting as the Dirac sea. Quantum fluctuations of the filled valence band are fierce, even leading to ultraviolet divergences; and one encounters such many-body phenomena as velocity renormalization,[5] screening of charge,[6] and nontrivial Coulombic corrections to cyclotron resonance.[7–11]

In multilayer graphene the zero-mode Landau levels acquire a new aspect. Bilayer graphene supports eight such levels, with an extra twofold degeneracy[1] in Landau orbitals n=0 and 1. Trilayer graphene has 12 such levels with threefold "orbital" degeneracy, and so on. This orbital degeneracy is a new feature peculiar to the LLL in multilayer graphene, and leads to intriguing quantum phenomena[12–17] such as orbital mixing and orbital-pseudospin waves. In real samples these zero-energy levels evolve, due to general interactions, into a variety of pseudo-zero-mode (PZM) levels, or broken-symmetry states within the LLL, as discussed theoretically.[12,18]

It has been unnoticed until recently that many-body effects work to lift orbital degeneracy. Each zero-mode level, subjected to quantum fluctuations of the valence band, gets shifted differently within the LLL, just like the Lamb shift[19] in the hydrogen atom. This orbital Lamb shift was first noted[20] for bilayer graphene and is also realized in an analogous fashion[21] in rhombohedral (ABC-stacked) trilayer graphene, which is a "chiral" trilayer generalization of bilayer graphene. This orbital shift is considerably larger in scale than intrinsic spin or valley breaking, and one has to take it into account in clarifying the fine structure of the LLL in multilayers.

Graphene trilayers attracted theorists' attention[22–25] even before experiments, and it has been verified experimentally[26–32] that the electronic properties of graphene trilayers strongly depend on the stacking order, with ABC-stacked trilayers exhibiting a tunable band gap and Bernal (ABA)-stacked trilayers, the most common type of trilayers, remaining metallic. Currently trilayers are under active study both experimentally[33,34] and theoretically.[35–39]

The purpose of this paper is to examine the orbital Lamb shift and its consequences in ABA-stacked trilayers, with focus on electron-hole and valley asymmetries due to general band parameters. It turns out that ABA trilayers critically differ in zero-mode characteristics from ABC trilayers. In particular, the way the Coulomb interaction acts within the LLL substantially differs between the two types of trilayers, leading to distinct basic filling-factor steps in which large level gaps appear in each of them. In addition, the LLL of ABA trilayers, unlike that of ABC trilayers, is greatly afflicted with interaction-enhanced electron-hole and valley asymmetries, which affect the sequence of broken-symmetry states within the LLL, observable via the quantum Hall effect.

In Sec. II we examine the one-body spectrum of the PZM levels in ABA-trilayer graphene, and in Sec. III show how the orbital Lamb shift modifies their full spectrum. In Sec. IV we discuss how the level spectra evolve, with filling, via the Coulomb interaction. Section VI is devoted to a summary and discussion on how ABA trilayers differ in zero-mode characteristics from ABC trilayers.

II. *ABA*-STACKED TRILAYER GRAPHENE

ABA-stacked trilayer graphene consists of three graphene layers with vertically-arranged dimer bonds (B_1, A_2) and (A_2, B_3), where (A_i, B_i) denote inequivalent lattice sites in the i-th layer. The interlayer coupling $\gamma_0 \equiv \gamma_{B_iA_i} \sim 3$ eV is related to the Fermi velocity $v = (\sqrt{3}/2)a_L\gamma_0/\hbar \sim 10^6$ m/s in monolayer graphene. Interlayer hopping via the nearest-neighbor dimer coupling $\gamma_1 \equiv \gamma_{B_1A_2} = \gamma_{A_2B_3} \sim 0.4$ eV leads to linear (monolayer-like) and quadratic (bilayer-like) spectra[22,23] $\propto |\mathbf{p}|, \mathbf{p}^2$ in the low-energy branches $|\epsilon| < \gamma_1$.

The effective Hamiltonian for *ABA*-stacked trilayer graphene with general intra- and interlayer couplings is written as[36]

$$\begin{aligned} H^{\rm tri} &= \int d^2\mathbf{x}\left[(\Psi^K)^\dagger\,\mathcal{H}_K\Psi^K + (\Psi^{K'})^\dagger\,\mathcal{H}_{K'}\,\Psi^{K'}\right], \\ \mathcal{H}_K &= \begin{pmatrix} D & V & W \\ V^\dagger & D & V^\dagger \\ W & V & D \end{pmatrix} + U,\ D = \begin{pmatrix} 0 & v\,p^\dagger \\ v\,p & 0 \end{pmatrix}, \\ V &= \begin{pmatrix} -v_4\,p^\dagger & v_3\,p \\ \gamma_1 & -v_4\,p^\dagger \end{pmatrix},\ W = \begin{pmatrix} \gamma_2/2 & 0 \\ 0 & \gamma_5/2 \end{pmatrix}, \\ U &= {\rm diag}(U_1, U_1+\Delta', U_2+\Delta', U_2, U_3, U_3+\Delta'), \end{aligned} \tag{1}$$

with $p = p_x + ip_y$ and $p^\dagger = p_x - ip_y$. Here $\Psi^K = (\psi_{A_1}, \psi_{B_1}, \psi_{A_2}, \psi_{B_2}, \psi_{A_3}, \psi_{B_3})^{\rm t}$ stands for the electron field at the K valley. v_3 and v_4 are related to the nonleading nearest-layer coupling $\gamma_3 \equiv \gamma_{A_1B_2}$ and $\gamma_4 \equiv \gamma_{A_1A_2} = \gamma_{B_1B_2}$, respectively. $\gamma_2 \equiv \gamma_{A_1A_3}$ and $\gamma_5 \equiv \gamma_{B_1B_3}$ describe coupling between the top and bottom layers. (U_1, U_2, U_3) denote the on-site energies of the three layers; we take $U_2 = 0$ without loss of generality and focus on the case of a symmetric bias[22] $U_3 = -U_1 \equiv u$. Such an interlayer bias leads to a tunable band gap for *ABC*-stacked trilayers, but not for *ABA*-stacked trilayers which involve monolayer-like subbands. Δ' stands for the energy difference between the dimer and non-dimer sites. $\mathcal{H}_K$ is diagonal in (suppressed) electron spin.

The Hamiltonian $\mathcal{H}_{K'}$ at another valley is given by $\mathcal{H}_K$ with $p \to -p_x + ip_y = -p^\dagger$ and $p^\dagger \to -p$, and acts on a spinor of the same sublattice content as Ψ^K. $\mathcal{H}_{K'}$ is not linked to $\mathcal{H}_K$ in a simple way and, in a magnetic field, their Landau-level spectra significantly differ,[35] especially for zero-mode levels, although they precisely but nontrivially[35] agree when only the leading parameters (v, γ_1) are kept. This is in sharp contrast to the case of bilayers and *ABC*-stacked trilayers, for which $\mathcal{H}_{K'}$ is linked to $\mathcal{H}_K$ via unitary equivalence,[20,21] such as $\mathcal{H}^{ABC}_{K'} \sim \mathcal{H}^{ABC}_K|_{-v_3,-\gamma_2;U_1\leftrightarrow U_3}$.

For the trilayer hopping parameters one may use, as typical values, those for graphite,[36]

$$\begin{aligned} &\gamma_0 \approx 3.16\,{\rm eV} \text{ or } v \approx 1.0\times 10^6{\rm m/s}, \\ &\gamma_1 \approx 0.4\,{\rm eV}, \gamma_3 \approx 0.3\,{\rm eV}, \gamma_4 \approx 0.04\,{\rm eV}, \\ &\gamma_2 \approx -0.02\,{\rm eV}, \gamma_5 \approx 0.04\,{\rm eV}, \Delta' \approx 0.05\,{\rm eV}. \end{aligned} \tag{2}$$

In the present analysis we regard (v, γ_1) as the basic parameters and treat the nonleading ones $(\gamma_2, \gamma_5, \gamma_4, \cdots)$ and bias u as perturbations. We ignore $v_3 \propto \gamma_3$ from the start since its effect is negligible in high magnetic fields, as discussed later in this section.

Let us place trilayer graphene in a strong uniform magnetic field $B_z = B > 0$ normal to the sample plane; we set, in $\mathcal{H}_K$, $p \to \Pi = p + eA$ with $A = A_x + iA_y = -B\,y$, and scale $a \equiv \sqrt{2eB}\,\Pi^\dagger$ so that $[a, a^\dagger] = 1$. It is easily seen that the eigenmodes of $\mathcal{H}_K$ have the structure

$$\begin{aligned} \Psi_n &= \Big(|n-2\rangle\, b_n^{(1)}, |n-1\rangle\, d_n^{(1)}, |n-1\rangle\, b_n^{(2)}, \\ &\qquad |n\rangle\, d_n^{(2)}, |n-2\rangle\, b_n^{(3)}, |n-1\rangle\, d_n^{(3)}\Big)^{\rm t} \end{aligned} \tag{3}$$

with $n = 0, 1, 2, \cdots$, where only the orbital eigenmodes are shown using the standard harmonic-oscillator basis $\{|n\rangle\}$ (with the understanding that $|n\rangle = 0$ for $n < 0$). The coefficients $\mathbf{v}_n = (b_n^{(1)}, d_n^{(1)}, b_n^{(2)}, d_n^{(2)}, b_n^{(3)}, d_n^{(3)})^{\rm t}$ are given by the eigenvectors (chosen to form an orthonormal basis) of the reduced Hamiltonian $\hat{\mathcal{H}}_{\rm red} \equiv \omega_c\mathcal{H}_n$ with

$$\mathcal{H}_n = \begin{pmatrix} -\hat{u} & r_{n-1} & -\lambda r_{n-1} & 0 & R_2 & 0 \\ r_{n-1} & \delta-\hat{u} & \hat{\gamma} & -\lambda r_n & 0 & R_5 \\ -\lambda r_{n-1} & \hat{\gamma} & \delta & r_n & -\lambda r_{n-1} & \hat{\gamma} \\ 0 & -\lambda r_n & r_n & 0 & 0 & -\lambda r_n \\ R_2 & 0 & -\lambda r_{n-1} & 0 & \hat{u} & r_{n-1} \\ 0 & R_5 & \hat{\gamma} & -\lambda r_n & r_{n-1} & \delta+\hat{u} \end{pmatrix}, \tag{4}$$

where $r_n \equiv \sqrt{n}$ for short; $\hat{u} \equiv u/\omega_c$, $\hat{\gamma} \equiv \gamma_1/\omega_c$. $\lambda \equiv \gamma_4/\gamma_0\,(\approx 0.013)$, $R_2 \equiv (\gamma_2/2)/\omega_c$, $R_5 \equiv (\gamma_5/2)/\omega_c$ and $\delta \equiv \Delta'/\omega_c$. Here

$$\omega_c \equiv \sqrt{2}\,v/\ell \approx 36.3\times v[10^6{\rm m/s}]\,\sqrt{B[{\rm T}]}\ {\rm meV} \tag{5}$$

stands for the characteristic cyclotron energy for monolayer graphene, with v in units of 10^6m/s and B in teslas; $\ell \equiv 1/\sqrt{eB}$ denotes the magnetic length. Note that eigenvectors $\mathbf{v}_n$ can be taken real since $\mathcal{H}_n$ is a real symmetric matrix.

Solving the secular equation shows that there are 6 branches of Landau levels for each integer $n \geq 2$, with two branches of monolayer-like spectra $\epsilon \sim \pm\sqrt{n-1}\,\omega_c$ and four branches of bilayer-like spectra. We denote the eigenvalues as $\epsilon_{-n''} < \epsilon_{-n'} < \epsilon_{-n} < 0 < \epsilon_n < \epsilon_{n'} < \epsilon_{n''}$, so that the index $\pm n$ reflects the sign of ϵ_n. The $|n| = 2$ levels, e.g., consist of the $n = (\pm 2.\pm 2', \pm 2'')$ branches.

As verified easily, with only (v, γ_1) and bias u kept, the spectrum and eigenvectors of $\hat{\mathcal{H}}_{\rm red}$ have the property

$$\epsilon_{-n} = -\epsilon_n|_{-u}, b_{-n}^{(i)} = -b_n^{(i)}|_{-u}, d_{-n}^{(i)} = d_n^{(i)}|_{-u}, \tag{6}$$

for $|n| \geq 2$ [and each branch (n, n', n'')], where $b_n^{(i)}|_{-u}$, e.g., stands for $b_n^{(i)}$ with $u \to -u$. This structure[40] is also seen from the fact that $-\mathcal{H}_K$ is unitarily equivalent to $\mathcal{H}_K$ with the signs of $(U_i, v_4, \gamma_2, \gamma_5, \Delta')$ reversed,

$$\Sigma_3^\dagger\mathcal{H}_K\Sigma_3 = -\mathcal{H}_K|_{-U_i,-v_4,-\gamma_2,-\gamma_5,-\Delta'}, \tag{7}$$

where $\Sigma_3 = \mathrm{diag}(\sigma_3, \sigma_3, \sigma_3)$; thus Eq. (6) is generalized to the full spectrum accordingly.

There are three zero-energy solutions (per spin) within the $n \in (0,1)$ sector for $u \to 0$. As seen from Eq. (3), for $n = 0$, $\hat{\mathcal{H}}_{\rm red}$ is reduced to a matrix of rank 1, with an obvious eigenvalue

$$\epsilon_0 = U_2 = 0 \tag{8}$$

and the eigenvector $\mathbf{v}_0 = (0,0,0,1,0,0)^{\rm t}$ or

$$\Psi_0 = (0,0,0,|0\rangle,0,0)^{\rm t}. \tag{9}$$

For $n = 1$, $\hat{\mathcal{H}}_{\rm red}$ has rank 4, and we specify the four eigenmodes as $n = 1_\pm$ and $n = \pm 1'$, with energy spectra $\epsilon_{1_\pm} = \pm\sigma\, u$ and $\epsilon_{\pm 1'} = \pm(1/\sigma)\,\omega_c \sim \pm\sqrt{2}\,\gamma_1$ when only (v, γ_1, u) are kept, where

$$\sigma \approx 1/\sqrt{2\,\hat{\gamma}^2 + 1}\ < 1; \tag{10}$$

$\hat{\gamma} \approx 2.4$ and $\sigma \approx 0.28$ at $B = 20\,\mathrm{T}$ with $\gamma_1 \approx 0.4\,\mathrm{eV}$. For $u \to +0$, in particular, the $n = 1_\pm$ modes have zero energy with wave functions

$$\begin{aligned}
\Psi^{(0)}_{1_+} &\overset{u\to 0}{=} \Big(0, \alpha^-|0\rangle, 0, c_1\,|1\rangle, 0, -\alpha^+|0\rangle\Big)^{\rm t},\\
\Psi^{(0)}_{1_-} &\overset{u\to 0}{=} \Big(0, -\alpha^+|0\rangle, 0, c_1\,|1\rangle, 0, \alpha^-|0\rangle\Big)^{\rm t},
\end{aligned} \tag{11}$$

where $\alpha^\pm \equiv (1 \pm \sigma)/2 \sim 1/2$ and $c_1 \equiv \sqrt{2\,\alpha^+\alpha^-} = \hat{\gamma}/\sqrt{2\hat{\gamma}^2+1} \sim 1/\sqrt{2}$.

When bias u and nonleading parameters $(\gamma_2, \gamma_5, \cdots)$ are turned on, the zero-modes Ψ_0 and $\Psi^{(0)}_{1_\pm}$ in general deviate from zero energy and become the pseudo-zero-modes. Their spectra, to first order in such perturbations, can also be determined using this $u \to 0$ zero-mode basis $\Psi^{\rm pz} = (\Psi_0, \Psi^{(0)}_{1_+}, \Psi^{(0)}_{1_-})^{\rm t}$. Writing $H^{\rm tri}$ in the 3×3 matrix form $\mathcal{H}^{\rm pz}_{ij} \sim (\Psi^{\rm pz})^\dagger_i \mathcal{H}_K (\Psi^{\rm pz})_j$ yields the spectrum of the pseudo-zero-mode (PZM) sector,

$$\begin{aligned}
\mathcal{H}^{\rm pz} &= \{0\} \oplus \mathcal{H}_1,\\
\mathcal{H}_1 &= \sigma u\,\sigma_3 + \beta_0\,1 + \beta\,\sigma_1,
\end{aligned} \tag{12}$$

where

$$\begin{aligned}
\beta &= \tfrac{1}{2}(1-c_1^2)\,\gamma_5 - c_1^2\,\Delta' + 2\,\sigma\,c_1\lambda\,\omega_c,\\
\beta_0 &= -\tfrac{1}{2}c_1^2\,\gamma_5 + (1-c_1^2)\,\Delta' + 2\,\sigma\,c_1\lambda\,\omega_c.
\end{aligned} \tag{13}$$

This PZM spectrum $\mathcal{H}^{\rm pz}$, in the framework of degenerate perturbation theory, is correct to order linear in $(u, \gamma_5, \lambda, \Delta')$, which is sufficient for our present purpose.

Diagonalizing $\mathcal{H}_1$ by a rotation within the $\{1_\pm\}$ sector,

$$\begin{aligned}
\Psi_{1_+} &= \cos(\theta/2)\,\Psi^{(0)}_{1_+} - \sin(\theta/2)\,\Psi^{(0)}_{1_-},\\
\Psi_{1_-} &= \sin(\theta/2)\,\Psi^{(0)}_{1_+} + \cos(\theta/2)\,\Psi^{(0)}_{1_-},
\end{aligned} \tag{14}$$

yields the eigenspectrum

$$\epsilon_{1_\pm} = \beta_0 \pm \sqrt{\beta^2 + \sigma^2 u^2} = \beta_0 \pm |\beta|/\sin\theta, \tag{15}$$

with $\sin\theta = 1/\sqrt{1 + \sigma^2u^2/\beta^2}$ and $\cot\theta = -\sigma u/\beta$; note that $\beta \approx -11.4\,\mathrm{meV} < 0$ and $\beta_0 \approx 18.6\,\mathrm{meV} > 0$ for the set (2) of parameters and at B =20 T. In particular, for $u \to +0$ ($\theta \to \pi/2$) the spectrum reads

$$\begin{aligned}
\epsilon_{1_+} &\overset{u\to 0}{=} \beta_0 + |\beta| = \Delta' - \tfrac{1}{2}\gamma_5\ (\sim 30\,\mathrm{meV}),\\
\epsilon_{1_-} &\overset{u\to 0}{=} (1-2c_1^2)\,(\tfrac{1}{2}\gamma_5 + \Delta') + 4\sigma c_1\lambda\,\omega_c,
\end{aligned} \tag{16}$$

which, for $\hat{\gamma} \to \infty$, recovers an earlier result,[36] with $c_1^2 \to 1/2$, $\sigma \to 0$ and $\epsilon_{1_-} \to 0$.

Here we wish to discuss possible effects of the interlayer coupling $\gamma_3 \equiv \gamma_{A_1B_2} \propto v_3$. It induces transitions that go outside the PZM sector, as one can verify using the solutions $(\Psi_0, \Psi_{1_\pm})$. Accordingly, its contributions to the spectra $(\epsilon_0, \epsilon_{1_\pm})$ are only of second order in v_3/v and are negligible in high magnetic fields.

The Hamiltonian $\mathcal{H}_{K'}$ at another valley is given by $\mathcal{H}_K$ with replacement $\Pi \leftrightarrow -\Pi^\dagger$. As for its spectrum one readily finds the following: The associated eigenmodes $\Psi^{K'}_n$ take the form of Ψ_n in Eq. (3), with replacement $|n\rangle \to |n-2\rangle$ for $d^{(2)}_n$ and $|n-2\rangle \to |n\rangle$ for $(b^{(1)}_n, b^{(3)}_n)$. The reduced Hamiltonian $\mathcal{H}_n|^{K'}$ is obtained from $\mathcal{H}_n$ in Eq. (4) by replacing each r_{n-1} by $-r_n$ and each r_n by $-r_{n-1}$. One, of course, has to calculate the eigenvectors $\mathbf{v}_n|^{K'} = (b^{(1)}_n, d^{(1)}_n, ...)^{\rm t}|^{K'}$ anew.

Unlike $\mathcal{H}_n$, $\mathcal{H}^{K'}_n$ has rank 2 for $n = 0$ and rank 5 for $n = 1$. This already signals that the PZM spectra significantly differ between the two valleys. For $n = 0$ one considers the 2×2 matrix Hamiltonian $\hat{\mathcal{H}}_{\rm red}|^{K'} \sim -u\,\sigma_3 + \frac{1}{2}\gamma_2\sigma_1$, with eigenmodes (denoted as $n = 0_\pm$),

$$\begin{aligned}
\Psi_{0_+} &= \big(-\sin(\phi/2)\,|0\rangle, 0, 0, 0, \cos(\phi/2)\,|0\rangle, 0\big)^{\rm t},\\
\Psi_{0_-} &= \big(\cos(\phi/2)\,|0\rangle, 0, 0, 0, \sin(\phi/2)\,|0\rangle, 0\big)^{\rm t},
\end{aligned} \tag{17}$$

and the associated spectra

$$\epsilon_{0_\pm} = \pm\sqrt{(\gamma_2/2)^2 + u^2} = \pm\tfrac{1}{2}|\gamma_2|/\sin\phi, \tag{18}$$

where $\sin\phi = 1/\sqrt{1 + (2u/\gamma_2)^2}$ and $\tan\phi = -\frac{1}{2}\gamma_2/u$.

For $n = 1$, $\mathcal{H}^{K'}_n$ has rank 5. Of its five eigenvalues, one belongs to the PZM sector, two are monolayer-like with $\epsilon_{\pm 1'} \sim \pm\omega_c$ and two are bilayer-like with $\epsilon_{\pm 1''} \sim \pm\sqrt{2}\gamma_1$. In the $u \to 0$ basis, the zero-energy mode is given by

$$\Psi_{n=1} \overset{u\to 0}{=} c_1\,(|1\rangle, 0, \kappa\,|0\rangle, 0, |1\rangle, 0)^{\rm t}, \tag{19}$$

where $\kappa \equiv 1/\hat{\gamma}$ and $c_1 \equiv \hat{\gamma}/\sqrt{2\hat{\gamma}^2+1} = 1/\sqrt{2+\kappa^2}$. Evaluating the expectation value $\epsilon_1 = \Psi_1^\dagger(\omega_c\,\mathcal{H}_{n=1}|^{K'})\Psi_1$ yields the spectrum of the $n = 1$ mode,

$$\epsilon_1 = c_1^2\,(\gamma_2 + 4\kappa\lambda\,\omega_c + \kappa^2\Delta'), \tag{20}$$

correct to order linear in $(u, \gamma_2, \gamma_5, v_4, \Delta')$ as well.

The LLL, i.e, the PZM sector, consists of $n \in (0, 1_\pm)$ at valley K and of $n \in (0_\pm, 1)$ at valley K'; there are thus twelve PZM levels differing in spin, valley and orbital. It is interesting to look into their structure. For zero bias

$u \to +0$ (i.e., $\theta = \phi \to \pi/2$), Ψ_0 and Ψ_{1_-} at valley K are predominantly composed of the orbital mode $|0\rangle$ and $|1\rangle$, respectively, residing on the B sites of the middle layer; let us denote this feature as $\Psi_0|^K \sim |0\rangle$ on B_2 and $\Psi_{1_-}|^K \sim |1\rangle$ on B_2. One can further write $\Psi_{1_+}|^K \sim |0\rangle$ on $B_{1,3}$, $\Psi_1|^{K'} \sim |1\rangle$ on $A_{1,3}$, $\Psi_{0_-}|^{K'} \sim |0\rangle$ on A_1, and $\Psi_{0_+}|^{K'} \sim |0\rangle$ on A_3. This naturally explains why ϵ_0 and ϵ_{1_-} are insensitive to the outer-layer coupling (γ_2, γ_5) and are less sizable. In this way, in ABA trilayers the PZM levels show valley asymmetry in composition.

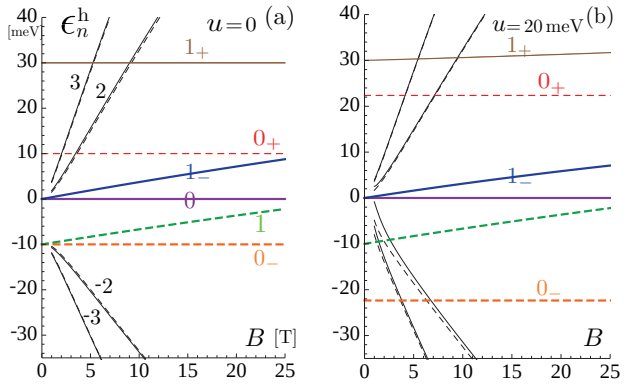

FIG. 1: (Color online) One-body level spectra $\epsilon_n^{\rm h}$ as a function of B for (a) $u = 0$ and (b) $u = 20$ meV. Real curves refer to valley K and dashed ones to valley K'.

The valley asymmetry is manifest in the one-body spectra $\{\epsilon_n\}$, which, from now on, are denoted as $\{\epsilon_n^{\rm h}\}$ to indicate that they come from $H^{\rm tri}$. Numerically, for $B = 20\,{\rm T}$ and with the set of parameters in Eq. (2) taken,

$$(\epsilon^{\rm h}_{1_+}, \epsilon^{\rm h}_{1_-}, \epsilon^{\rm h}_0) \overset{u\to 0}{\approx} (30, 7.15, 0)\,{\rm meV},$$
$$(\epsilon^{\rm h}_{0_+}, \epsilon^{\rm h}_1, \epsilon^{\rm h}_{0_-}) \overset{u\to 0}{\approx} (10, -3.64, -10)\,{\rm meV}. \quad (21)$$

Figure 1 shows the spectra $\{\epsilon_n^{\rm h}\}$ for $u = (0, 20)$ meV as a function of magnetic field B, along with the $n = \pm 2, \pm 3$ bilayer-like spectra. The PZM sector is considerably spread in energy $\sim \Delta' - \frac{1}{2}(\gamma_5 + \gamma_2) \sim 40\,{\rm meV}$, but, for large $B > 15\,{\rm T}$, it is practically isolated from other levels. The PZM spectra prominently differ between the two valleys (real curves *vs* dashed ones). In addition, they are highly electron-hole (eh) asymmetric (i.e., not symmetric about zero energy) and this eh asymmetry comes from $\beta_0 \neq 0$ and $\epsilon_1 \neq 0$, i.e., primarily from (γ_5, Δ') at valley K and γ_2 at valley K'. Note that $\epsilon^{\rm h}_{1_\pm}$ and $\epsilon^{\rm h}_{0_\pm}$ vary with interlayer bias u. Practically only $\epsilon^{\rm h}_{0_\pm}$ vary sensitively with u while other levels are barely affected.

Let us now make the Landau-level structure explicit by passing to the $|n, y_0\rangle$ basis $\ni \{\Psi_n\}$ with $y_0 \equiv \ell^2 p_x$ via the expansion $(\Psi^K(\mathbf{x}), \Psi^{K'}(\mathbf{x})) = \sum_{n,y_0} \langle \mathbf{x}|n, y_0\rangle \{\psi^{n;a}_\alpha(y_0)\}$, where n refers to the level index, $\alpha \in (\uparrow, \downarrow)$ to the spin, and $a \in (K, K')$ to the valley. The charge density $\rho_{-\mathbf{p}} = \int d^2\mathbf{x}\, e^{i\mathbf{p}\cdot\mathbf{x}}\, \rho$ with $\rho = (\Psi^K)^\dagger \Psi^K + (\Psi^{K'})^\dagger \Psi^{K'}$ is thereby written as[20]

$$\rho_{-\mathbf{p}} = \gamma_{\mathbf{p}} \sum_{k,n=-\infty}^{\infty} \sum_{a,\alpha} g^{kn;a}_{\mathbf{p}}\, R^{kn;aa}_{\alpha\alpha;\mathbf{p}},$$
$$R^{kn;ab}_{\alpha\beta;\mathbf{p}} \equiv \int dy_0\, \psi^{k,a\,\dagger}_\alpha(y_0)\, e^{i\mathbf{p}\cdot\mathbf{r}}\, \psi^{n,b}_\beta(y_0), \quad (22)$$

where $\gamma_{\mathbf{p}} \equiv e^{-\ell^2\mathbf{p}^2/4}$; $\mathbf{r} = (i\ell^2\partial/\partial y_0, y_0)$ denotes the center coordinate with $[r_x, r_y] = i\ell^2$.

The coefficient matrix $g^{kn;a}_{\mathbf{p}} \equiv g^{kn}_{\mathbf{p}}|^a$ at valley $a \in (K, K')$ is constructed from the eigenvectors $\mathbf{v}_n|^a$,

$$g^{kn}_{\mathbf{p}}|^K = \{b^{(1)}_k b^{(1)}_n + b^{(3)}_k b^{(3)}_n\}\, f^{|k|-2,|n|-2}_{\mathbf{p}} + \{d^{(1)}_k d^{(1)}_n + b^{(2)}_k b^{(2)}_n + d^{(3)}_k d^{(3)}_n\}\, f^{|k|-1,|n|-1}_{\mathbf{p}} + d^{(2)}_k d^{(2)}_n\, f^{|k|,|n|}_{\mathbf{p}}, \text{etc.}, \quad (23)$$

and has the property $(g^{mn;a}_{\mathbf{p}})^\dagger = g^{n,m;a}_{-\mathbf{p}}$. Here

$$f^{kn}_{\mathbf{p}} = \sqrt{n!/k!}\,(-\bar{q}/\sqrt{2})^{k-n}\, L_n^{(k-n)}(|\bar{q}|^2/2) \quad (24)$$

for $k \geq n \geq 0$, and $f^{nk}_{\mathbf{p}} = (f^{kn}_{-\mathbf{p}})^\dagger$; $\bar{q} = \ell(p_x - i\,p_y)$; it is understood that $f^{kn}_{\mathbf{p}} = 0$ for $k < 0$ or $n < 0$.

Within the PZM sector,

$$g^{00}_{\mathbf{p}} = 1,\ g^{01_\pm}_{\mathbf{p}} = (\cos\tfrac{\theta}{2} \mp \sin\tfrac{\theta}{2})\, c_1 \ell\, p/\sqrt{2},$$
$$g^{1_\pm 1_\pm}_{\mathbf{p}} = 1 - (1 \mp \sin\theta)\tfrac{1}{2}(c_1)^2\, \ell^2\mathbf{p}^2,$$
$$g^{1_+ 1_-}_{\mathbf{p}} = g^{1_- 1_+}_{\mathbf{p}} = -(\cos\theta)\,\tfrac{1}{2}(c_1)^2\, \ell^2\mathbf{p}^2, \quad (25)$$

at valley K, and

$$g^{0_+ 0_+}_{\mathbf{p}} = g^{0_- 0_-}_{\mathbf{p}} = 1,\quad g^{0_+ 0_-}_{\mathbf{p}} = 0,$$
$$g^{0_\pm 1}_{\mathbf{p}} = (\cos\tfrac{\phi}{2} \mp \sin\tfrac{\phi}{2})\, c_1 \ell\, p/\sqrt{2},$$
$$g^{11}_{\mathbf{p}} = 1 - (c_1)^2\, \ell^2\mathbf{p}^2, \quad (26)$$

at valley K', with $c_1 = 1/\sqrt{2 + \kappa^2}$ and $\kappa \equiv 1/\hat{\gamma}$. One can further show that, with only (v, γ_1, u) kept, these $g^{kn}_{\mathbf{p}}$ are only corrected to $O(\hat{u}^2\kappa^2)$ or smaller.

In view of Eqs. (6) and (7), the form factors $g^{mn;a}_{\mathbf{p}}$ enjoy the property

$$g^{mn;a}_{\mathbf{p}} = g^{-m,-n;a}_{\mathbf{p}}|_{-U_i, -v_4, -\gamma_2, -\gamma_5, -\Delta'} \quad (27)$$

for general (m, n), where it is understood that one sets $\pm m \to j$ for the PZM level j. This property plays a key role in our analysis later. Equations (25) and (26) are expressions valid to zero*th* order in perturbations $(u, \gamma_2, \gamma_5, \cdots)$, but they actually know the nature of perturbations through the mixing angles (θ, ϕ) that depend on the relative strengths $(u/\beta, u/\gamma_2)$. They indeed satisfy Eq. (27).

The form factors $g^{kn}_{\mathbf{p}}$ generally differ between the two valleys. Interestingly, they happen to coincide for $u \to 0$: Indeed, for $u \to 0$, one finds

$$g^{1_+ 1_+}_{\mathbf{p}} = g^{00}_{\mathbf{p}} = 1, g^{1_- 1_-}_{\mathbf{p}} = 1 - c_1^2\ell^2\mathbf{p}^2,$$
$$g^{01_+}_{\mathbf{p}} = g^{1_- 1_+}_{\mathbf{p}} = 0, g^{01_-}_{\mathbf{p}} = c_1\, \ell\, p, \quad (28)$$

at valley K, and analogous K'-valley expressions with $(1_+, 1_-, 0)$ replaced by $(0_+, 1, 0_-)$ in the above. This fact tells us that the charge $\rho_{\mathbf{p}}$ takes a manifestly valley-symmetric form for zero bias $u = 0$ while the one-body spectra $\{\epsilon_n^{\rm h}\}$ inevitably break valley symmetry. In addition, Eq. (28) implies that, for $u \to 0$, $1_+|^K$ is isolated from $(0, 1_-)|^K$, and similarly, $0_+|^{K'}$ from $(1, 0_-)|^{K'}$.

From now on we frequently suppress summations over levels n, spins α and valleys a, with the convention that the sum is taken over repeated indices. The Hamiltonian $H^{\rm tri}$ projected to the PZM sector is thereby written as

$$H^{\rm h} = \epsilon_n^{\rm h}\, R^{nn}_{\alpha\alpha;\mathbf{p}=\mathbf{0}} - \mu_{\rm Z}\,(T_3)_{\beta\alpha} R^{nn}_{\alpha\beta;\mathbf{p}=\mathbf{0}} \tag{29}$$

with $n \in (0, 1_\pm, 0_\pm, 1)$. Here the Zeeman term $\mu_{\rm Z} \equiv g^*\mu_{\rm B} B \approx 0.12\, B[{\rm T}]$ meV is introduced via the spin matrix $T_3 = \sigma_3/2$. Actually, the Zeeman energy $\mu_{\rm Z}$ is only about 3 meV even at $B = 30$ T and is generally smaller than energy splitting due to valley breaking. Accordingly, in what follows, we mostly suppose that the spin is practically unresolved and focus on energy gaps due to valley and orbital breaking.

III. VACUUM FLUCTUATIONS

In this section we examine the effect of Coulombic quantum fluctuations on the PZM multiplet. The Coulomb interaction is written as

$$V = \tfrac{1}{2}\textstyle\sum_{\mathbf{p}} v_{\mathbf{p}}\ :\rho_{-\mathbf{p}}\,\rho_{\mathbf{p}}:, \tag{30}$$

where $v_{\mathbf{p}} = 2\pi\alpha/(\epsilon_{\rm b}|\mathbf{p}|)$ with $\alpha = e^2/(4\pi\epsilon_0) \approx 1/137$ and the substrate dielectric constant $\epsilon_{\rm b}$. For simplicity we ignore the difference between the intralayer and interlayer Coulomb potentials.

In this paper we generally study many-body ground states $|G\rangle$ with a homogeneous density, realized at integer filling factor $\nu \in [-6, 6]$. We set the expectation values $\langle G|R^{mn;ab}_{\alpha\beta;\mathbf{k}}|G\rangle = \delta_{\mathbf{k},\mathbf{0}}\,\rho_0\,\nu^{mn;ab}_{\alpha\beta}$ with $\rho_0 = 1/(2\pi\ell^2)$, so that the filling factor $\nu^{nn;aa}_{\alpha\alpha} = 1$ for a filled (n, a, α) level.

Let us define the Dirac sea $|{\rm DS}\rangle$ as the valence band with levels below the PZM sector (i.e., levels with $n \le -2$, $n' \le -1'$, ...) all filled. We construct the Hartree-Fock Hamiltonian $V^{\rm HF} = V_{\rm D} + V_{\rm X}$ out of V as the effective Hamiltonian that governs the electron states over $|{\rm DS}\rangle$. As usual, the direct interaction $V_{\rm D}$ is removed if one takes into account the neutralizing positive background. We thus focus on the exchange interaction

$$V_{\rm X} = -\sum_{\mathbf{p}} v_{\mathbf{p}}\gamma_{\mathbf{p}}^2\, g^{mn';b}_{-\mathbf{p}}\, g^{m'n;a}_{\mathbf{p}}\, \nu^{mn;ba}_{\beta\alpha}\, R^{m'n';ab}_{\alpha\beta;\mathbf{0}}, \tag{31}$$

where we sum over filled levels (m, n) and retain the PZM sector $m', n' \in (0, 1_\pm, 0_\pm, 1)$.

Let us first extract the contribution from the Dirac sea,

$$V_{\rm X}^{\rm DS} = -\sum_{\mathbf{p}} v_{\mathbf{p}}\gamma_{\mathbf{p}}^2 \sum_{n\in{\rm DS}} |g^{m'n;a}_{\mathbf{p}}|^2\, R^{m'm';aa}_{\alpha\alpha;\mathbf{0}}, \tag{32}$$

where the sum is understood over spin α and over $m' \in (0, 1_\pm)$ for $a = K$ and $m' \in (0_\pm, 1)$ for $a = K'$. Actually, the sum over infinitely many filled levels with $n \in {\rm DS}$ gives rise to an ultraviolet divergence.

Fortunately this infinite sum is evaluated exactly to zero*th* order in perturbations $(u, \gamma_2, \gamma_5, \cdots)$, as done earlier,[20,21] if one notes Eq. (27) and the completeness relation[20]

$$\sum_{n=-\infty}^{\infty} |g^{mn;a}_{\mathbf{p}}|^2 = e^{\ell^2\mathbf{p}^2/2} \ \text{ for each } a \in (K, K'). \tag{33}$$

The result is

$$\sum_{n\in{\rm DS}} |g^{jn;K}_{\mathbf{p}}|^2 = \frac{1}{2}\,(e^{\ell^2\mathbf{p}^2/2} - |g^{j0}_{\mathbf{p}}|^2 - |g^{j1_+}_{\mathbf{p}}|^2 - |g^{j1_-}_{\mathbf{p}}|^2), \tag{34}$$

for $j \in (0, 1_\pm)$; analogously for valley K'. The $e^{\ell^2\mathbf{p}^2/2}$ term leads to a divergence upon integration over $\mathbf{p}$; it, however, shifts all levels j uniformly and is safely omitted. The regularized Dirac-sea contribution then reads

$$\begin{aligned} V_{\rm X}^{\rm DS}\ {}^{0^{th}}\!\!= {}& \epsilon_0^{\rm v}\, R^{00}_{\alpha\alpha;\mathbf{0}} + \epsilon_{1_+}^{\rm v}\, R^{1_+1_+}_{\alpha\alpha;\mathbf{0}} + \epsilon_{1_-}^{\rm v}\, R^{1_-1_-}_{\alpha\alpha;\mathbf{0}} \\ & + \epsilon_{0_+}^{\rm v}\, R^{0_+0_+}_{\alpha\alpha;\mathbf{0}} + \epsilon_{0_-}^{\rm v}\, R^{0_-0_-}_{\alpha\alpha;\mathbf{0}} + \epsilon_1^{\rm v}\, R^{11}_{\alpha\alpha;\mathbf{0}}, \\ \epsilon_j^{\rm v} = {}& \frac{1}{2}\sum_{\mathbf{p}} v_{\mathbf{p}}\gamma_{\mathbf{p}}^2 \sum_{n\in(0,1_\pm)} |g^{jn}_{\mathbf{p}}|^2 \ \text{for } j \in (0, 1_\pm); \end{aligned} \tag{35}$$

analogously for $j \in (0_\pm, 1)$. Integration over $\mathbf{p}$, with the formula $\sum_{\mathbf{p}} v_{\mathbf{p}}\gamma_{\mathbf{p}}^2\,[1, (\ell|\mathbf{p}|)^2, (\ell|\mathbf{p}|)^4] = [1, 1, 3]\,\tilde{V}_c$, yields

$$\begin{aligned} \epsilon_0^{\rm v} &= \tfrac{1}{2}\,(1 + c_1^2)\,\tilde{V}_c, \\ \epsilon_{1_\pm}^{\rm v} &= \tfrac{1}{2}\big[1 - (1 \mp \sin\theta)\,\tfrac{1}{2}(c_1^2 - 3c_1^4)\big]\,\tilde{V}_c, \\ \epsilon_{0_\pm}^{\rm v} &= \tfrac{1}{2}\,\big[1 + \tfrac{1}{2}c_1^2(1 \mp \sin\phi)\big]\,\tilde{V}_c, \\ \epsilon_1^{\rm v} &= \tfrac{1}{2}\,(1 - c_1^2 + 3\,c_1^4)\,\tilde{V}_c, \end{aligned} \tag{36}$$

where $c_1^2 \equiv (c_1)^2$, etc., $\tilde{V}_c \equiv \sqrt{\pi/2}\,V_c$ and

$$V_c \equiv \alpha/(\epsilon_b\ell) \approx (56.1/\epsilon_b)\,\sqrt{B[{\rm T}]}\,{\rm meV}. \tag{37}$$

Note that Eqs. (34) $\sim$ (36) are the zeroth-order expressions, which depend on bias u through the zero*th*-order ratios $\sin\phi$ and $\sin\theta$. Numerically, for $u = 0$ and $B = 20$ T, and with $\epsilon_b = 5$ taken as a typical value,

$$\begin{aligned} \epsilon_0^{\rm v} &= \epsilon_{0_-}^{\rm v} = \tfrac{1}{2}\,(1 + c_1^2)\,\tilde{V}_c \approx 0.73\,\tilde{V}_c, \\ \epsilon_{1_-}^{\rm v} &= \epsilon_1^{\rm v} = \tfrac{1}{2}(1 - c_1^2 + 3\,c_1^4)\,\tilde{V}_c \approx 0.59\,\tilde{V}_c, \\ \epsilon_{1_+}^{\rm v} &= \epsilon_{0_+}^{\rm v} = \tfrac{1}{2}\,\tilde{V}_c = 0.5\,\tilde{V}_c. \end{aligned} \tag{38}$$

In this way, the PZM levels are "Lamb-shifted" due to vacuum fluctuations and the splitting among $\{\epsilon_j^{\rm v}\}$ reflects the difference in their spatial (or $\mathbf{p}$) distributions.

In Fig. 2 the Lamb shifts $\{\epsilon_j^{\rm v}\}$ are plotted, in units of $\tilde{V}_c$, as a function of bias u. They are ordered, e.g., as $\epsilon_0^{\rm v} > \epsilon_{1_-}^{\rm v} > \epsilon_{1_+}^{\rm v}$ at one valley, and are valley-symmetric

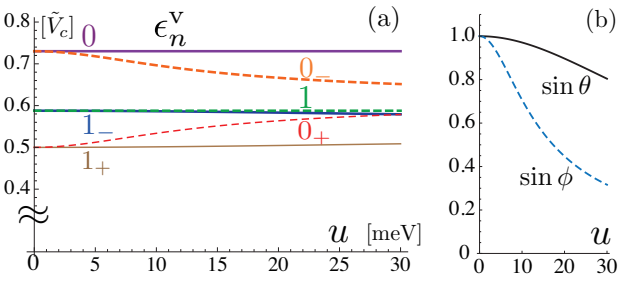

FIG. 2: (Color online) (a) Orbital Lamb-shift corrections $\{\epsilon_j^{\rm v}\}$ plotted in units of $\tilde{V}_c$ as a function of bias u at $B = 20\,{\rm T}$. (b) $\sin\theta$ and $\sin\phi$ as a function of u for $B = 20\,{\rm T}$.

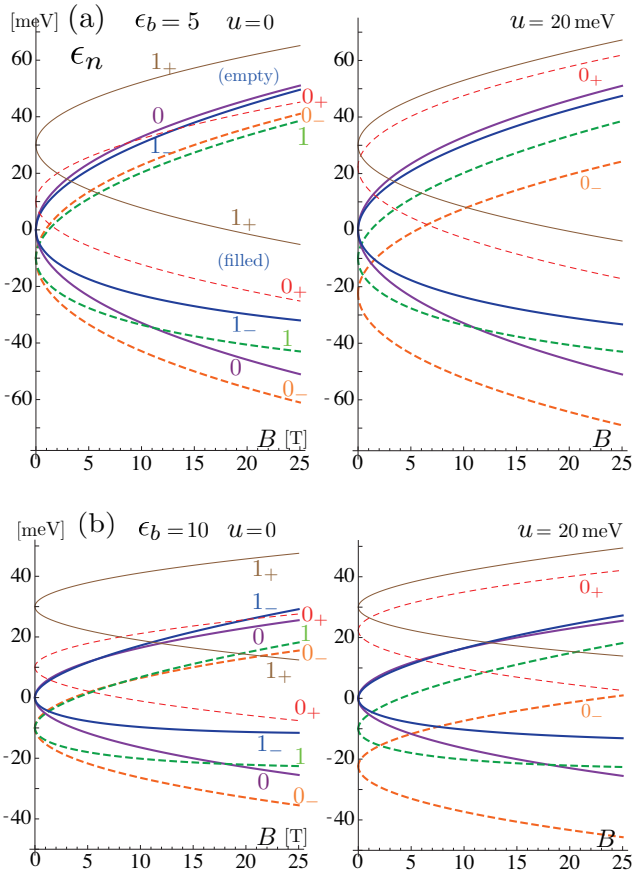

FIG. 3: (Color online) Level spectra of the empty and filled PZM sector. (a) $\epsilon_b = 5$ and $u = (0, 20)$ meV. The upper and lower halves of each parabolic spectrum refer to the empty ($\nu = -6$) and filled ($\nu = 6$) case, respectively. (b) $\epsilon_b = 10$ and $u = (0, 20)$ meV, with a weaker Coulomb potential.

for $u = 0$ (this reflects the manifest valley symmetry of the charge $\rho_{\mathbf{p}}$ noted in Sec. II), with valley asymmetry developing gradually with increasing bias u.

The spectra (36) or (38) refer to those of empty levels. Actually the spectra vary (i.e., generally go down due to the exchange interaction) with filling of the PZM levels. In particular, Eq. (32) tells us that, when the PZM sector is filled up, $\{\epsilon_j^{\rm v}\}$ change sign $\epsilon_j^{\rm v} \to -|\epsilon_j^{\rm v}|$. In this sense, the Lamb-shift corrections $\{\epsilon_j^{\rm v}\}$ preserve eh symmetry. Thus, as the PZM sector is filled from $\nu = -6$ (empty) to $\nu = 6$ (full), the spectrum of the j-th level varies from $\epsilon_j^{\rm h} + \epsilon_j^{\rm v}$ to $\epsilon_j^{\rm h} - \epsilon_j^{\rm v}$. See Fig. 3(a), which depicts the (empty/filled) spectra $\epsilon_j^{\rm h} \pm \epsilon_j^{\rm v}$ as a function of B, for $u = 0$ and $\epsilon_{\rm b} = 5$; the upper and lower halves of each spectrum refer to empty and filled levels, respectively. Note that bias u works to enhance the splitting of the $0_\pm$ spectra. For reference, Fig. 3(b) shows the level spectra for a weaker potential with $\epsilon_{\rm b} = 10$.

At valley K, the one-body spectra $\{\epsilon_n^{\rm h}\}$ are ordered so that $\epsilon_{1_+}^{\rm h} > \epsilon_{1_-}^{\rm h} > \epsilon_0^{\rm h}$ while $\{\epsilon_n^{\rm v}\}$ are ordered so that $\epsilon_0^{\rm v} > \epsilon_{1_-}^{\rm v} > \epsilon_{1_+}^{\rm v}$. The Lamb-shift contributions $\{\epsilon_n^{\rm v}\}$ therefore enhance splitting among filled levels $(1_+, 1_-, 0)$ with spectra $\epsilon_n^{\rm h} - \epsilon_n^{\rm v}$. For empty levels (with $\epsilon_n^{\rm h} + \epsilon_n^{\rm v}$) they work oppositely and even reverse the ordering of the 1_- and 0 spectra when the Coulomb interaction $\tilde{V}_c$ is strong enough (i.e., for smaller ϵ_b and higher B); compare Figs. 3(a) and 3(b). Replacing $(1_+, 1_-, 0) \to (0_+, 1, 0_-)$ also allows one to find essentially the same features for valley K'. In this way the Lamb-shift contributions, though eh symmetric by themselves, work to enhance eh asymmetry in the full PZM spectra $\epsilon_j^{\rm h} \pm \epsilon_j^{\rm v}$.

To see how each level evolves with filling, one has to examine the Coulomb interaction acting within the LLL; we study this in the next section.

IV. COULOMB INTERACTIONS

The Coulomb exchange interaction acting within the PZM sector is written as

$$V_{\rm X}^{\rm pz} = -\tilde{V}_c\, \Gamma_{\beta\alpha}^{n'm'}\, R_{\alpha\beta;\mathbf{0}}^{m'n'}, \tag{39}$$

with $\Gamma_{\beta\alpha}^{n'm'} \equiv \sum_{\mathbf{p}} v_{\mathbf{p}} \gamma_{\mathbf{p}}^2\, (g_{\mathbf{p}}^{n'm})^*\, g_{\mathbf{p}}^{m'n}\, \nu_{\beta\alpha}^{mn}/\tilde{V}_c = \Gamma_{\alpha\beta}^{m'n'}$, where (m', n') and (m, n) are summed over $(0, 1_\pm, 0_\pm, 1)$. For definiteness we focus on the $u \to 0$ case, where $g_{\mathbf{p}}^{mn}$ and $\Gamma_{\beta\alpha}^{n'm'}$ considerably simplify. Indeed, as noted in Eq. (28), for $u = 0$, the charge $\rho_{\mathbf{p}}$ takes a valley-symmetric form and, in addition, one has $g_{\mathbf{p}}^{01_+} = g_{\mathbf{p}}^{1_-1_+} = 0$ and $g_{\mathbf{p}}^{0_+0_-} = g_{\mathbf{p}}^{0_+1} = 0$. This structure suggests that, at valley K, 1_+ tends to be isolated from $(0, 1_-)$ which may potentially get mixed; similarly, 0_+ tends to be isolated from $(0_-, 1)$ at valley K'. Actually, for $u = 0$ one finds that

$$\begin{aligned}
&\Gamma^{00} = \nu^{00} + \nu^{1_-1_-}\, c_1^2, \\
&\Gamma^{1_-1_-} = \nu^{00}\, c_1^2 + \nu^{1_-1_-}\, (1 - 2c_1^2 + 3c_1^4), \\
&\Gamma^{01_-} = \nu^{01_-}\, (1 - c_1^2),\ \Gamma^{1_+1_-} = \nu^{1_+1_-}\, (1 - c_1^2), \\
&\Gamma^{1_+1_+} = \nu^{1_+1_+},\ \Gamma^{01_+} = \nu^{01_+},
\end{aligned} \tag{40}$$

at valley K, with obvious spin indices (α, β) suppressed. Replacing $(0, 1_-, 1_+) \to (0_-, 1, 0_+)$ in the above yields expressions $\Gamma^{K'K'}$ for valley K' and, in an analogous way, mixed-valley components $\Gamma^{KK'}$ as well. One can further

use new orbital labels $\hat{n}$ and rename $(0, 1_-, 1_+)$ as $(\hat{1}, \hat{2}, \hat{3})$ with valley $a = K$, and $(0_-, 1, 0_+)$ as $(\hat{1}, \hat{2}, \hat{3})$ with valley $a = K'$, so that, e.g., $\nu^{00} = \nu^{\hat{1}\hat{1};KK}$, $\nu^{00_-} = \nu^{\hat{1}\hat{1};KK'}$, etc. Then the exchange interaction $V_{\rm X}^{\rm pz}$ itself is cast into a valley- (and spin-)symmetric form composed of terms like $\nu^{\hat{n}\hat{m};ba}_{\beta\alpha}\, R^{\hat{m}'\hat{n}';ab}_{\alpha\beta;\mathbf{0}}$.

The PZM levels are now governed by the effective Hamiltonian $\mathcal{V} \equiv H^{\rm h} + V_{\rm X}^{\rm DS} + V_{\rm X}^{\rm pz}$. Note first that the interaction $V_{\rm X}^{\rm DS} + V_{\rm X}^{\rm pz}$ is symmetric in spin and valley (for $u = 0$). Thus $\mathcal{V}$ is made diagonal in valley and spin if one takes the valley basis (K, K') and the spin basis $(\uparrow, \downarrow)$ of the one-body part $H^{\rm h} \sim \{\epsilon_n^{\rm h}\}$. Accordingly, one can treat each valley and spin separately, and diagonalize $\mathcal{V}$ with respect to the orbital modes $(0, 1_-, 1_+)|^K$ and $(0_-, 1, 0_+)|^{K'}$ for each spin.

Let us now discuss how the PZM levels evolve with filling. For definiteness, we first suppose filling the empty PZM sector with electrons gradually under a fixed magnetic field $B = 20\,\mathrm{T}$ and $u = 0$. We consider 6 levels, $(0, 1_\pm, 0_\pm, 1)$ per spin, and use $0 \le n_{\rm f} \le 6$ to denote the filling factor for this subsector; with electron spins supposed to be unresolved, the PZM sector thereby has the filling factor $\nu = 2(n_{\rm f} - 3)$. (We refer to the case of resolved spins later.) Our focus is on uniform ground states at integer filling. To follow their evolution, we choose to diagonalize the Hamiltonian $\mathcal{V}$ with uniform states at intermediate filling factors; this serves to visualize how level mixing and crossing take place, as we shall see.

One can read from Fig. 3(a) the level spectra of the empty/filled PZM sector,

$$\begin{aligned} &(\ \epsilon_1,\ \ \epsilon_{0_-},\ \ \epsilon_{0_+},\ \epsilon_{1_-},\ \ \epsilon_0,\ \ \epsilon_{1_+}) \\ &\overset{\text{empty}}{\approx}\ (33.3, 35.9, 41.4, 44.1, 45.9, 61.4)\ \text{meV}, \\ &\overset{\text{filled}}{\to}\ -(40.6, 55.9, 21.4, 29.8, 45.9, 1.44)\ \text{meV}, \end{aligned} \tag{41}$$

where $\epsilon_n|^{\text{empty/filled}} = \epsilon_n^{\rm h} \pm \epsilon_n^{\rm v}$ and $\epsilon_b = 5$. It is seen from these spectra that the $1|^{K'}$ and $0_-|^{K'}$ levels potentially have crossing, so do $0|^K$ and $1_-|^K$. This signals level mixing within each pair.

It is the lowest-lying $1|^{K'}$ level that starts to be filled first. As it is filled, it cooperates with the $0_-|^{K'}$ level, paired via the exchange interaction. To clarify how they evolve, one can now try to diagonalize $\mathcal{V} = H^{\rm h} + V_{\rm X}^{\rm DS} + V_{\rm X}^{\rm pz}$ for the three lowlying levels $(1, 0_-, 0_+)|^{K'}$, and subsequently for those at valley K. See the appendix for an analysis.

Figure 4(a) summarizes the resulting evolution of level spectra. For $0 \le n_{\rm f} \le n_{\rm cr}$ with $n_{\rm cr} \approx 0.145$ only the $1|^{K'}$ level is filled and gets lower in energy along with the (paired) empty $0_-|^{K'}$ level. Beyond $n_{\rm cr}$, $1|^{K'}$ is mixed with $0_-|^{K'}$ and turns into $0_-|^{K'}$ at $n_{\rm f} \approx 1.145$; at the same time, $0_-|^{K'}$ turns into $1|^{K'}$. Both $0_-|^{K'}$ and $1|^{K'}$ levels are eventually filled up at $n_{\rm f} = 2$. At integer filling $n_{\rm f} = 1$, the $(1, 0_-)$-mixed levels consist of a filled level of energy ≈ -27.0 meV and an empty level of energy ≈ 7.0 meV. A close look into Fig. 4(a) reveals that an "orbital" rotation takes place so as to avoid level crossing. The remaining $0_+|^{K'}$ level evolves individually, and is filled over the interval $n_{\rm f} \in [2, 3]$.

For $n_{\rm f} > 3$ an analogous process is repeated for $(1_-, 0, 1_+)|^K$ levels at another valley. There mixing of

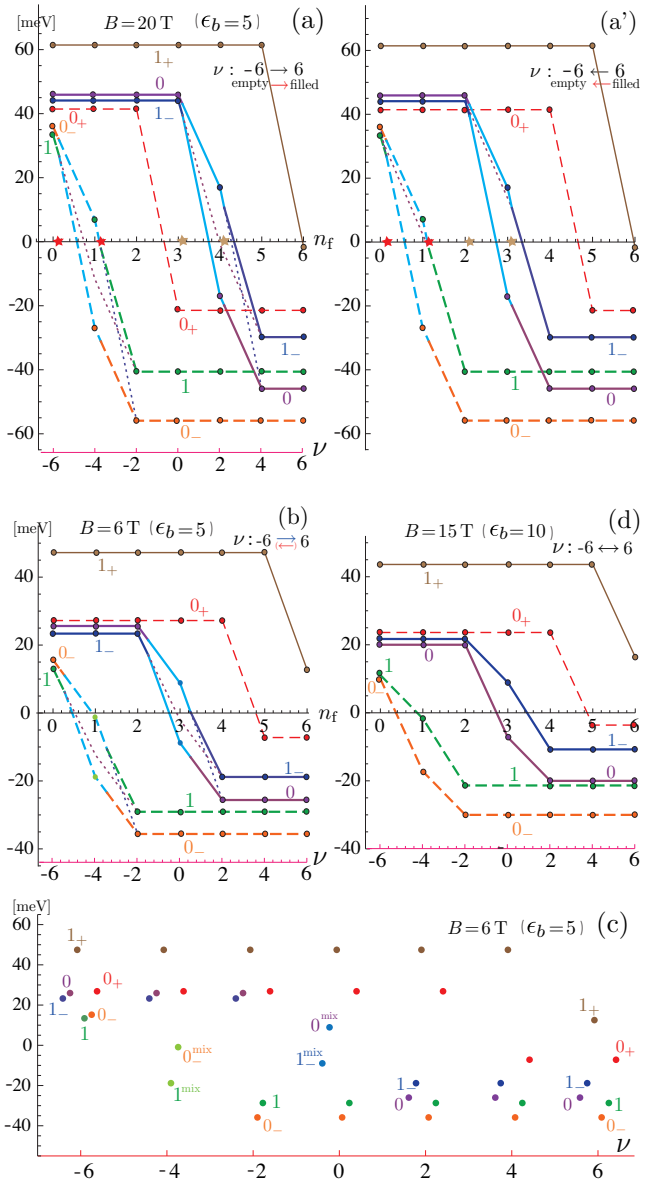

FIG. 4: (Color online) (a) Evolution of level spectra at $B = 20\,\mathrm{T}$ and $\epsilon_b = 5$ as the PZM sector is filled from $n_{\rm f} = 0$ (empty) to $n_{\rm f} = 6$ (full); the filling factor $\nu = 2(n_{\rm f} - 3) \in [-6, 6]$, with the electron spin supposed to be unresolved. Orbital mixing takes place over the interval $n_{\rm f} \in (0.145, 1.145)$ and $n_{\rm f} \in (3.101, 4.101)$, indicated by colored stars. Thin dotted curves represent evolution of level spectra when no orbital rotation were allowed. (a') Evolution of level spectra when the PZM sector is emptied from $n_{\rm f} = 6$ to $n_{\rm f} = 0$. (b) and (c) Level spectra for $B = 6\,\mathrm{T}$ and $\epsilon_b = 5$. (d) Level mixing is absent for a weaker Coulomb potential with $\epsilon_b = 10$ and at $B = 15\,\mathrm{T}$.

$1_-|^K$ and $0|^K$ takes place over the interval $n_{\rm f} \in (n'_{\rm cr}, 1+n'_{\rm cr})$ with $n'_{\rm cr} \approx 3.101$, and avoids level crossing.

From Fig. 4(a) one can read off the spectra of the PZM sector at each integer filling factor $\nu \in [-6, 6]$. The spectra are *eh*- and valley-asymmetric. Let us now note that, due to this *eh* asymmetry, the level spectra may evolve in a different pattern when one empties the PZM sector rather than filling it. Indeed, such a difference is clearly seen from Fig. 4(a'), which shows the evolution of level spectra when the filled PZM sector is gradually emptied (i.e., $\nu = 6 \to -6$) under the same $B = 20\,{\rm T}$. Actually, Fig. 4(a') is a result of direct calculation, but it will be clear how to draw it by a glance at Fig. 4(a).

For comparison, see also Figs. 4(b) and 4(c), which show the evolution of level spectra under $B = 6\,{\rm T}$. There the pattern of evolution is uniquely fixed, independent of whether one fills or empties the PZM sector. Lastly, Fig. 4(d) illustrates the case of a weaker Coulomb potential with $\epsilon_{\rm b} = 10$ and at $B = 15\,{\rm T}$, corresponding to the level spectra in Fig. 3(b). Here again the pattern of level spectra is uniquely fixed, but, unlike in the above cases, there is no level mixing.

In general, the level spectra $\epsilon^{\rm h}_j \pm \epsilon^{\rm v}_j$ of the empty/filled PZM sector (in Fig. 3) are fixed in advance by specifying the value of magnetic field B at $\nu = -6$ and $\nu = 6$, respectively. How the spectra evolve at intermediate filling factors, as we have seen, depends on whether one fills or empties the PZM sector and how one does it, e.g., under fixed B or fixed density $\rho \propto \nu B$.

It will be clear from the model calculations above that the $1_+|^K$ and $0_+|^{K'}$ levels evolve individually without mixing with others while $1_-|^K$ and $0|^K$ move in pairs, so do $(1, 0_-)|^{K'}$. Actually, with this experience, a close look into the empty/filled spectra in Fig. 3 allows one to draw a general idea about how the level spectra evolve under fixed B and $u = 0$ (or even for small u as well).

For example, the presence or absence of level mixing is inferred from Fig. 3. Level mixing takes place so as to avoid crossing of paired levels $(1_-, 0)|^K$ or $(1, 0_-)|^{K'}$. As noted in Sec. II, the ordering of these paired levels, i.e., $\epsilon^{\rm h}_{1_-} > \epsilon^{\rm h}_0$ and $\epsilon^{\rm h}_1 > \epsilon^{\rm h}_{0_-}$ for $\epsilon^{\rm h}_n$, is reversed for the full spectra $\epsilon^{\rm h}_n + \epsilon^{\rm v}_n$ when the Coulomb potential $\tilde{V}_c \sim \alpha/(\epsilon_b \ell)$ is strong enough. It is thus this inversion of (empty) paired levels that drives level mixing. Accordingly, with $\epsilon_{\rm b} = 5$, mixing of paired levels is necessarily present for almost all values of B in Fig. 3(a), as indeed seen from Figs. 4(a) and 4(b). For Fig. 3(b), i.e., for a weaker potential with $\epsilon_{\rm b} = 10$, mixing is present only at low $B \lesssim 7\,{\rm T}$ and is absent at higher B, as is the case with Fig. 4(d). When bias u is turned on, mixing of $(1, 0_-)|^{K'}$ disappears rapidly with increasing u, but mixing of $(1_-, 0)|^K$ tends to persist at low B, as verified easily.

In the level spectra of Fig. 3, the $0_+|^{K'}$ level is relatively isolated upward from the paired levels $(1, 0_-)|^{K'}$, so is $1_+|^K$ from $(1_-, 0)|^K$. It is therefore the lowest-lying $(1, 0_-)|^{K'}$ pair that is filled first as $n_{\rm f} = 0 \to 2$ (or emptied last as $n_{\rm f} = 2 \to 0$). This leads to a unique $\nu = -2$ ground state [consisting of filled $(1, 0_-)|^{K'}$ levels] with a relatively large $\nu = -2$ level gap, as is evident from Fig. 4. Likewise, an isolated $1_+|^K$ level leads to a unique $\nu = 4$ state with a relatively large gap. The ground states at other filling factors, in contrast, vary in composition case by case. In particular, one notices an equally large $\nu = 2$ gap and a relatively small $\nu = 0$ gap in the spectra of Figs. 4(b) and 4(d), which show essentially the same low-B characteristics of the PZM sector [at $B \lesssim 10\,{\rm T}$ in Fig. 3(a) or $\lesssim 20\,{\rm T}$ in Fig. 3(b)]. Interestingly, in those low-B cases, the $\nu = 0$ state (essentially) consists of filled $(0, 1, 0_-)$ levels, which is the same in composition as the $\nu = 0$ state one naively expects from the one-body spectra $\{\epsilon^{\rm h}_n\}$ in Fig. 1 alone.

We have so far supposed unresolved electron spins. Note that the exchange interaction acts on pairs of the same spin and valley. Accordingly, if, e.g., in Fig. 4(b), there were two $(1, 0_-)|^{K'}$ pairs of spin up and down resolved against possible disorder, each pair would repeat the $n_{\rm f} = 0 \to 2$ evolution in the figure over the interval $\nu = -6 \to -4 \to -2$, yielding a $\nu = -4$ gap comparable to the $\nu = -2$ gap. In this way, small spin gaps, if resolved, are equally well enhanced by the interaction, and will modify the evolution patterns in Fig. 4 accordingly.

The transport properties of graphene trilayers have been studied in a number of experiments,[26–34] and some nontrivial features of the LLL of *ABA*-stacked trilayers have been observed. Evidence for the opening of the $\nu = 0$ gap comes from early observations[26,30] of an insulating $\nu = 0$ state in both *ABA* and *ABC* trilayers.

Recent experiments on substrate-supported *ABA* trilayer graphene by Henriksen *et al.*[33] observed a robust $\nu = -2$ Hall plateau and a possible incipient $\nu = 2$ or $\nu = 4$ plateau under zero bias ($u \sim 0$), and $\nu = \pm 2, \pm 4$ plateaus in biased samples. Subsequent measurements on dual-gated suspended devices by Lee *et al.*[34] observed $\nu = \pm 2$ plateaus at low magnetic field $B < 4\,{\rm T}$ and also resolved, in high magnetic fields, additional plateaus at $\nu = \pm 1, \pm 3, -4$, and -5, indicating almost complete lifting of the 12-fold degeneracy of the LLL. Common to these observations, in particular, is *eh* asymmetry in the sequence of plateaus, with a prominent $\nu = -2$ plateau.

The $B = 6\,{\rm T}$ and $\epsilon_b = 5$ case of Fig. 4(b) appears to capture these features seen in experiment at low B. For resolved spins, this case will lead to large gaps at $\nu = \pm 2, \pm 4$, 0, 3 and 5, and relatively small gaps at $\nu = \pm 1$, -3 and -5. In our picture, appreciable *eh* asymmetry is a result of Coulombic enhancement of the *eh* asymmetry in $H^{\rm h}$ and a large $\nu = -2$ gap is triggered by the valley asymmetry of $H^{\rm h}$ such that $\min[\epsilon^{\rm h}_{0_-}, \epsilon^{\rm h}_1]^{K'} < \min[\epsilon^{\rm h}_0, \epsilon^{\rm h}_{1_-}]^K$, i.e., the K' valley is relatively lower in spectrum. In general, large level gaps are associated with evolution of orbital modes $(1_-, 0)|^K$ and $(1, 0_-)|^{K'}$ of basic filling step $\Delta n_{\rm f} = 2$ per spin and evolution of rather independent modes $1_+|^K$ and $0_+|^{K'}$ of step $\Delta n_{\rm f} = 1$. This is in sharp contrast to the case of *ABC* trilayers, where large gaps within the LLL are associated with evolution (actually, mixing) of orbital modes of ba-

sic step[21] $\Delta n_{\rm f}=3$ per spin, leading to visible $\nu=0,\pm3$ plateaus.

V. SUMMARY AND DISCUSSION

In a magnetic field graphene trilayers develop, as the LLL, a multiplet of twelve nearly-zero-energy levels with a three-fold orbital degeneracy. In this paper we have examined the quantum characteristics of this PZM multiplet in ABA trilayers, with the Coulomb interaction and the orbital Lamb shift taken into account. It turned out that ABA trilayers are distinct in zero-mode characteristics from ABC trilayers examined earlier.[21] We have, in particular, seen that both valley and eh symmetries are markedly broken in the LLL of ABA trilayers. These asymmetries appear in the one-body spectra $\{\epsilon_n^{\rm h}\}$ already to first order in nonleading hopping parameters (such as γ_2, γ_5 and Δ'), and are enhanced via the Lamb-shift contributions $\{\epsilon_n^{\rm v}\}$ and the Coulomb interaction acting within the LLL.

In contrast, for ABC trilayers the one-body PZM spectra $\{\epsilon_n^{\rm h}\}$ involve, for zero bias $u=0$, only a tiny eh asymmetry of $O(v_4)\sim O(v_4\omega_c/v\tilde\gamma)$ and no valley breaking[41] linear in nonleading parameters (γ_2,γ_3,v_4). The Lamb-shift corrections $\{\epsilon_n^{\rm v}\}$ add no further breaking (to the leading order). Accordingly, in ABC trilayers the LLL is far less afflicted by eh and valley asymmetries.

The PZM levels differ in structure between the two types of trilayers. In ABA trilayers they are composed of the $|0\rangle$ and $|1\rangle$ orbital modes distributed in a distinct way at each valley, as noted in Sec. II, and in this sense the associated valley asymmetry is intrinsic. In contrast, in ABC trilayers these levels are characterized by the $|0\rangle$, $|1\rangle$ and $|2\rangle$ orbital modes residing predominantly on one of the outer layers,[21] with the two valleys related symmetrically [by layer and site interchange $(A_1,B_1)\leftrightarrow(B_3,A_3)$].

The two types of trilayers substantially differ in the way the Coulomb interaction acts within the LLL. They thus differ in the way large level gaps or the associated conductance plateaus appear within the LLL, with ABA trilayers having basic filling steps of $\Delta n_{\rm f}=(2,1)$ and ABC trilayers having a step of $\Delta n_{\rm f}=3$.

Interlayer bias u also acts quite differently on the two types of trilayers. For ABC trilayers, u acts oppositely at the two valleys and enhances valley gaps. In contrast, for ABA trilayers, it works to further split $\epsilon_{0_\pm}|^{K'}$ (and $\epsilon_{1_\pm}|^{K}$), i.e., enhance orbital breaking at each valley.

The orbital Lamb shift is a many-body vacuum effect but is intimately correlated with the Coulomb interaction acting within the multiplet. This is clear if one notes that the filled PZM sector and the empty one, both subject to quantum fluctuations of the filled valence band, differ by the amount of this Coulomb interaction. It will be clear now why this vacuum effect, though it could easily be overlooked if one naively relies on the Coulomb interaction projected to the LLL alone, has to be properly taken into account in every attempt to explore the PZM sector in graphene few-layers.[42]

The eh and valley asymmetries inherent to ABA trilayers substantially modify the electron and hole spectra within the LLL. The sequence of broken-symmetry states, observable via the quantum Hall effect, is thereby both eh- and valley-asymmetric and can change in pattern, depending on how one fills or empties the LLL. We have presented some model calculations in Sec. IV, assuming a typical set (2) of parameters and ϵ_b. They are intended to illustrate what would generally happen when the orbital Lamb shift and Coulomb interactions are properly taken into account. They will also be a good base point for a more elaborate analysis when more data on graphene trilayers become available via future experiments.

Acknowledgments

This work was supported in part by a Grant-in-Aid for Scientific Research from the Ministry of Education, Science, Sports and Culture of Japan (Grant No. 24540270).

Appendix A: Evolution of level spectra

In this appendix we diagonalize the effective hamiltonian $\mathcal{V}\equiv H^{\rm h}+V_{\rm X}^{\rm DS}+V_{\rm X}^{\rm pz}$ for the three lowlying levels $(0_+,0_-,1)|^{K'}$, with the electron spin kept frozen. Let us write $\mathcal{V}=H^{mn}R^{mn}_{\mathbf{p}=\mathbf{0}}$ and $H^{mn}\equiv(\epsilon_n^{\rm h}+\epsilon_n^{\rm v})\,\delta^{mn}-\tilde V_c\,\Gamma^{nm}$, with $m,n\in(1,2,3)$ for $(0_+,0_-,1)$. Note that Γ^{mn} are real for real filling factors ν^{mn}, which we take. It therefore suffices to use a real $O(3)$ rotation to diagonalize the 3×3 real symmetric matrix H^{mn}. We thus rotate ψ^m in orbital $(0_+,0_-,1)$ space, $\psi^m=\mathcal{U}^{mn}\,\phi^n$, with three Euler angles $(\theta_3,\theta_2,\theta_1)$ parameterizing

$$\mathcal{U}=e^{-i\theta_3\,t_3}e^{-i\theta_2\,t_2}e^{-i\theta_1\,t_1},\tag{A1}$$

where the spin-1 generators $(t_a)^{bc}\equiv i\epsilon^{bac}$ in terms of the totally antisymmetric tensor ϵ^{abc} with $\epsilon^{123}=1$. Note that θ_1 mixes $n=(2,3)$, θ_2 mixes $(1,3)$, etc. We make $\mathcal{H}=\mathcal{U}^\dagger H\,\mathcal{U}$ diagonal, using the filling factors $\nu^{mn}=(\mathcal{U}^{mn'})^*N_{n'}\mathcal{U}^{nn'}$ expressed in terms of the filling fraction $N_n=(N_1,N_2,N_3)$ of the diagonalized levels ϕ^n.

Let us start filling the empty PZM sector at (relative) filling factor $n_{\rm f}=0$. Obviously, it is the lowest-lying $1|^{K'}$ level that starts to be filled. To follow how it evolves let us suppose that it is filled with fraction $n_{\rm f}\le1$ and set $(N_1,N_2,N_3)=(0,0,n_{\rm f})$. $\mathcal{H}^{mn}$ is diagonalized if one can adjust $\{\theta_n\}$ so that $\mathcal{H}^{12}=\mathcal{H}^{13}=\mathcal{H}^{23}=0$.

The onset of possible rotations is seen from the behavior of these $(\mathcal{H}^{12},\mathcal{H}^{13},\mathcal{H}^{23})$ under small rotations. To first order in $\{\theta_n\}$,

$$\begin{aligned}\mathcal{H}^{12}&\approx-(5.526+28.95\,n_{\rm f})\,\theta_3+\cdots,\\ \mathcal{H}^{13}&\approx(8.124+11.03\,n_{\rm f})\,\theta_2+\cdots,\\ \mathcal{H}^{23}&\approx(-2.597+17.91\,n_{\rm f})\,\theta_1+\cdots.\end{aligned}\tag{A2}$$

This structure reveals that $\{\theta_n\} = 0$ for $0 \le n_{\rm f} < n_{\rm cr}$ with $n_{\rm cr} \approx 2.597/17.91 \approx 0.145$ while $\theta_1 \neq 0$ is possible for $n_{\rm f} > n_{\rm cr}$. Solving for $\{\theta_n\}$ numerically shows that the energy eigenvalue $\mathcal{H}^{33}$ is indeed lowered for $n_{\rm f} > n_{\rm cr}$ with $\theta_1 \neq 0$ and $\theta_2 = \theta_3 = 0$. A further analysis reveals that θ_1 rises from 0 to $\pi/2$ for $n_{\rm c} \le n_{\rm f} \le n_{\rm c}^{+} \approx 1.145$ and then keeps $\pi/2$ up to $n_{\rm f} = 2$. (For $1 \le n_{\rm f} \le 2$ we set $(N_1, N_2, N_3) = (0, n_{\rm f} - 1, 1)$ and extend the solution across $n_{\rm f} = 1$.) Thus, over the interval $n_{\rm f} \in (n_{\rm cr}, n_{\rm cr}^{+})$ a rotation takes place in orbital space, and thereby the $1|^{K'}$ and $0_-|^{K'}$ levels are interchanged. Finally, the remaining 0_+ level is filled individually for $2 < n_{\rm f} \le 3$.

A similar analysis is also made for the $(1_+, 0, 1_-)|^K$ levels at another valley. The resulting evolution of level spectra is summarized in Fig. 4(a).

[1] E. McCann and V. I. Fal'ko, Phys. Rev. Lett. **96**, 086805 (2006).
[2] T. Ohta, A. Bostwick, T. Seyller, K. Horn, and E. Rotenberg, Science **313**, 951 (2006).
[3] E. McCann, Phys. Rev. B **74**, 161403(R) (2006).
[4] E. V. Castro, K. S. Novoselov, S. V. Morozov, N. M. R. Peres, J. M. B. Lopes dos Santos, J. Nilsson, F. Guinea, A. K. Geim, and A. H. Castro Neto, Phys. Rev. Lett. **99**, 216802 (2007).
[5] J. González, F. Guinea, and M. A. H. Vozmediano, Nucl. Phys. B **424**, 595 (1994).
[6] T. Misumi and K. Shizuya, Phys. Rev. B **77**, 195423 (2008).
[7] Z. Jiang, E. A. Henriksen, L. C. Tung, Y.-J. Wang, M. E. Schwartz, M. Y. Han, P. Kim, and H. L. Stormer, Phys. Rev. Lett. **98**, 197403 (2007).
[8] A. Iyengar, J. Wang, H. A. Fertig, and L. Brey, Phys. Rev. B **75**, 125430 (2007).
[9] Yu. A. Bychkov and G. Martinez, Phys. Rev. B **77**, 125417 (2008).
[10] S. Viola Kusminskiy, D. K. Campbell, and A. H. Castro Neto, Europhys. Lett. **85**, 58005 (2009).
[11] K. Shizuya, Phys. Rev. B **81**, 075407 (2010); **84**, 075409 (2011).
[12] Y. Barlas, R. Côté, K. Nomura, and A. H. MacDonald, Phys. Rev. Lett. **101**, 097601 (2008).
[13] K. Shizuya, Phys. Rev. B **79**, 165402 (2009).
[14] Y. Barlas, R. Côté, J. Lambert, and A. H. MacDonald, Phys. Rev. Lett. **104**, 096802 (2010).
[15] R. Côté, J. Lambert, Y. Barlas, and A. H. MacDonald, Phys. Rev. B **82**, 035445 (2010).
[16] R. Côté, W. Luo, B. Petrov, Y. Barlas, and A. H. MacDonald, Phys. Rev. B **82**, 245307 (2010).
[17] R. Côté, J. P. Fouquet, and W. Luo, Phys. Rev. B **84**, 235301 (2011).
[18] R. Nandkishore and L. Levitov, Phys. Rev. B **82**, 115124 (2010);
E. V. Gorbar, V. P. Gusynin, Junji Jia, and V. A. Miransky, Phys. Rev. B **84**, 235449 (2011).
[19] W. E. Lamb and R. C. Retherford, Phys. Rev. **72**, 241 (1947).
[20] K. Shizuya, Phys. Rev. B **86**, 045431 (2012).
[21] K. Shizuya, Phys. Rev. B **87**, 085413 (2013).
[22] F. Guinea, A. H. Castro Neto, and N. M. R. Peres, Phys. Rev. B **73**, 245426 (2006).
[23] M. Koshino and T. Ando, Phys. Rev. B **76**, 085425 (2007).
[24] J. Nilsson, A. H. Castro Neto, F. Guinea, and N. M. R. Peres, Phys. Rev. B **78**, 045405 (2008).
[25] M. Koshino and E. McCann, Phys. Rev. B **79**, 125443 (2009).
[26] W. Bao, Z. Zhao, H. Zhang, G. Liu, P. Kratz, L. Jing, J. Velasco, Jr., D. Smirnov, and C. N. Lau, Phys. Rev. Lett. **105**, 246601 (2010).
[27] A. Kumar, W. Escoffier, J. M. Poumirol, C. Faugeras, D. P. Arovas, M. M. Fogler, F. Guinea, S. Roche, M. Goiran, and B. Raquet, Phys. Rev. Lett. **107**, 126806 (2011).
[28] T. Taychatanapat, K. Watanabe, T. Taniguchi, and P. Jarilloo-Herrero, Nat. Phys. **7**, 621 (2011).
[29] C. H. Lui, Z. Li, K. F. Mak, E. Cappelluti, and T. F. Heinz, Nat. Phys. **7**, 944 (2011).
[30] W. Bao, L. Jing, J. Velasco Jr, Y. Lee, G. Liu, D. Tran, B. Standley, M. Aykol, S. B. Cronin, D. Smirnov, M. Koshino, E. McCann, M. Bockrath, and C. N. Lau, Nat. Phys. **7**, 948 (2011).
[31] L. Zhang, Y. Zhang, J. Camacho, M. Khodas, and I. Zaliznyak, Nat. Phys. **7**, 953 (2011).
[32] S. H. Jhang, M. F. Craciun, S. Schmidmeier, S. Tokumitsu, S. Russo, M. Yamamoto, Y. Skourski, J. Wosnitza, S. Tarucha, J. Eroms, and C. Strunk, Phys. Rev. B **84**, 161408(R) (2011).
[33] E. A. Henriksen, D. Nandi, and J. P. Eisenstein, Phys. Rev. X **2**, 011004 (2012).
[34] Y. Lee, J. Velasco, Jr, D. Tran, F. Zhang, W. Bao, L. Jing, K. Myhro, D. Smirnov, and C. N. Lau, Nano Lett. **13**, 1627 (2013).
[35] M. Koshino and E. McCann, Phys. Rev. B **81**, 115315 (2010).
[36] M. Koshino and E. McCann, Phys. Rev. B **83**, 165443 (2011).
[37] F. Zhang, B. Sahu, H. Min, and A. H. MacDonald, Phys. Rev. B **82**, 035409 (2010).
[38] S. Yuan, R. Roldan and M. I. Katsnelson, Phys. Rev. B **84**, 125455 (2011).
[39] F. Zhang, D. Tilahun, and A. H. MacDonald, Phys. Rev. B **85**, 165139 (2012).
[40] Actually, owing to the symmetry of ABA trilayers (under the interchange of layer $1 \leftrightarrow$ layer 3), the full spectrum of $\mathcal{H}_n$ is a function of $|u|$, i.e., $\epsilon_n = \epsilon_n|_{\pm u}$.
[41] The energy difference Δ between the dimer and nondimer sites was left out earlier, but one can show that Δ induces eh asymmetry but no valley asymmetry to $O(\Delta)$.
[42] Recently, the possibility of mixing of the PZM levels with levels in the velence band has been discussed for chiral multilayers; see C. Töke, arXiv:1309.5747v3.